Appl Phys A (2011) 102: 785–789
DOI 10.1007/s00339-011-6265-8

Applied Physics A
Materials Science & Processing

Metal/TiO_2 interfaces for memristive switches

J. Joshua Yang · John Paul Strachan · Feng Miao · Min-Xian Zhang · Matthew D. Pickett · Wei Yi · Douglas A.A. Ohlberg · G. Medeiros-Ribeiro · R. Stanley Williams

Received: 1 October 2010 / Accepted: 22 December 2010 / Published online: 26 January 2011

Abstract The interfaces between metal electrodes and the oxide in TiO_2-based memristive switches play a key role in the switching as well as in the I–V characteristics of the devices in different resistance states. We demonstrate here that the work function of the metal electrode has a surprisingly minor effect in determining the electronic barrier at the interface. In contrast, Ti oxides can be readily reduced by most electrode metals. The amount of oxygen vacancies created by these chemical reactions essentially determines the electronic barrier at the device interfaces.

The memristor, the fourth fundamental passive circuit element [1–3], has a wide variety of potential applications based on its promising device properties [1–7], including non-volatility, fast switching (<10 ns), low energy (∼1 pJ/operation), multiple-state operation, scalability and stackability. As suggested by the name, memristors can be used for information storage [8–14]. Moreover, memristors can function as stateful Boolean logic gates via the material implication operation [15]. In addition, memristors can also be used for neuromorphic computing [16, 17] because of their analog switching, and some hybrid circuits due to their ease of stacking [18, 19].

Among all the kinds of switching materials that have been reported, oxides are the most extensively studied [4]. The interfaces between the metal electrodes and the oxide play a crucial role, especially for bipolar switches [5, 6, 20]. Under an applied electric field, oxygen vacancies can drift into the interface region, reducing the electronic barrier and resulting in a low-resistance state. Under an electric field with the opposite polarity, the oxygen vacancies are repelled away from the interface region, recovering the electronic barrier to regain the high resistance state [6, 21, 22]. A family of nanodevices with different switching and current–voltage (I–V) characteristics has been demonstrated by manipulating the elemental composition at the two interfaces of a simple metal/oxide/metal device stack [23]. For a crossbar array of memristors in a storage/memory circuit, sneak path currents [24] can be minimized by using memristors with a rectifying I–V characteristic, especially when they are in the low-resistance state. Therefore, interface engineering is critical to obtain the desired switching behavior and electrical properties for memristive devices.

From a semiconductor physics point of view, the work function of the electrode metal might be an important factor in determining the electronic barrier at the metal/oxide interface [25]. This barrier in our thin film devices is not a traditional Schottky barrier because the oxide film is amorphous with a large concentration of defects and likely thinner than the depletion region of the semiconducting oxide. We prepared a set of 5 μm × 5 μm cross-point devices with six different top electrode metals (Au, Pt, Ag, Ni, W and Ti) to examine the effect of these contacts on the I–V characteristics, as shown in Fig. 1(a)–(f). The samples were simple crossbars with the stack shown in Fig. 1(g). The bottom electrodes of 5 nm Ti/15 nm Pt were evaporated on Si/200 nm SiO_2 substrates through a metal shadow mask. Then a blank TiO_2 layer of 25 nm was sputter deposited at a substrate temperature 270°C. During the deposition of the TiO_2 layer, the Ti adhesion layer diffused through the bottom Pt electrode at the elevated deposition temperature, reached the Pt/TiO_2 interface, reacted with the TiO_2 layer and created a significant

J.J. Yang (✉) · J.P. Strachan · F. Miao · M.-X. Zhang · M.D. Pickett · W. Yi · D.A.A. Ohlberg · G. Medeiros-Ribeiro · R.S. Williams
Hewlett-Packard Co, 1501 Page Mill Rd., Palo Alto, CA 94304-1100, USA
e-mail: jianhuay@hp.com

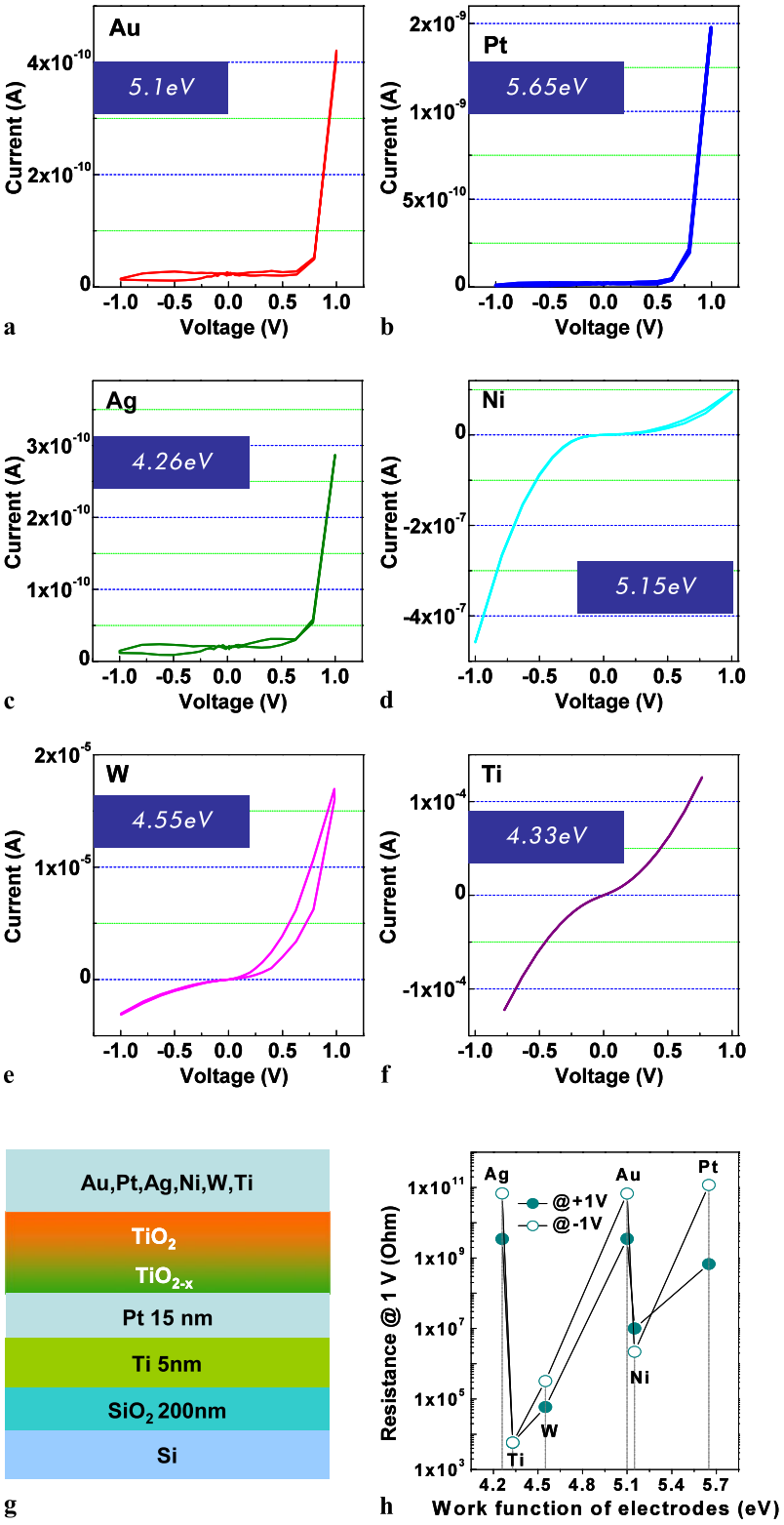

Fig. 1 (**a**)–(**f**) *I*–*V* curves of the TiO_2 devices with Au, Pt, Ag, Ni, W and Ti as the top electrodes, respectively. (**g**) Schematic of the device stack and (**h**) the plot of device resistance at ±1 V vs. the work function of the top electrode metal

amount of oxygen vacancies that made the bottom Pt/TiO_2 interface fairly conductive [26]. This bottom interface remained conductive during all the electrical testing, and the more resistive top interfaces dominated the electronic transport in these devices. On the same wafer with the stack of Si/200 nm SiO_2/5 nm Ti/15 nm Pt/25 nm TiO_2, 30 nm of the six metals were evaporated through a metal shadow mask to form the top electrodes at ambient temperature. No pho-

tolithography process was involved in the device fabrication in order to minimize the chemical contamination and obtain clean interfaces for comparison.

The I–V curves shown in Fig. 1(a)–(f) were taken with -1 V to $+1$ V quasi-DC sweeps on the top electrodes, while the bottom electrodes were grounded. The work function value (adopted for polycrystalline metal materials [27]) of each top electrode is indicated in the I–V plots in Fig. 1. Since not all the samples measured here can yield a meaningful Schottky barrier height (SBH) [28] by data fitting, the resistance instead of the SBH of the samples is used for comparison across all the samples with different metal electrodes. No clear relation can be seen between the resistances of the devices and the work function values of the top electrode metals. For example, Ag has the lowest work function among these metals, but the device with a Ag top electrode has one of the highest resistance values. In order to clearly demonstrate this point, a plot is made between the work function and the resistances of the each device at both $+1$ V and -1 V in Fig. 1(h), where no trend is apparent.

Thus, the electronic barrier at these metal/oxide interfaces is not dominated by the work function of the electrode metals, which can be explained by the presence of a high concentration of interface states that are intrinsic to the oxide surfaces or are caused by the metal deposition [29, 30]. Interface chemical reactions [31, 32] between the metal electrodes and the Ti oxide can be a major source of these interface states. The Ellingham diagram [33] is a useful tool, if used properly, to predict the possibility that reactions may occur. For example, one may expect that Cr cannot reduce TiO_2 based on the fact that the free energy of formation of Cr_2O_3 is above that of TiO_2 in the Ellingham diagram, as shown in Fig. 2(a). In fact, Cr can chemically reduce TiO_2 and create oxygen vacancies in the TiO_2 layer [26]. The reason is that there are many other phases in the Ti–O system, such that Cr does not have to reduce the oxide all the way to Ti metal, and the full set of intermediate oxide phases are not shown in a normal Ellingham diagram. For instance, the free energy of formation of TiO_2 from Ti_3O_5 and oxygen is above the formation free energy of Cr_2O_3 in the Ellingham diagram (Fig. 2(a)), and therefore Cr can reduce TiO_2 to Ti_3O_5.

There are many Magnéli phases with the formula Ti_nO_{2n-1} in the Ti–O system, where Magnéli phases from Ti_4O_7 up to $Ti_{20}O_{39}$ have already been discovered [34]. The free energy of formation of TiO_2 from the Magnéli phases approaches zero with increasing n as shown in Fig. 2(b). Therefore, in a complete Ellingham diagram with all the Ti–O phases, there could be a TiO_2 formation reaction from a Ti_nO_{2n-1} phase lying well above the formation reaction of most metal oxides, including NiO, WO_3 or even PtO_2, and oxygen vacancies in TiO_2 can thus be induced by Ni, W or even Pt metal electrodes. Even a very small amount of oxygen vacancies, less than 0.05%, is large enough as native dopants to reduce the resistivity of TiO_2 by orders of magnitude [35]. Since Au does not have a stable oxide (positive formation free energy) and the standard free energy of formation of sliver oxide is close to zero, almost no reduction occurs at the interfaces of TiO_2 with these metal electrodes, leading to the most resistive devices with these two metal electrodes in the studied sample set. In Fig. 2(c), the resistances of the devices at both $+1$ V and -1 V are plotted vs. the standard free energy of formation of the electrode metal oxides, where an approximately monotonic trend can be seen. The larger the formation free energy of the metal electrode oxide, the smaller the resistance of the device with that metal electrode. This suggests that the interface reaction between the top metal electrode and the TiO_2 is related to the observed difference in the I–V characteristics of the device set.

To complete our study and confirm the above description, we investigated the role that interfacial vacancies have on the I–V characteristics. For this purpose, a TiO_2 single crystal (rutile) was used to provide a cleaner, more well-defined system. The crystal was annealed in vacuum (10^{-8} Torr) at 600°C for 30 min to introduce a small amount of oxygen vacancies. The annealed rutile crystal turned from transparent to light blue and became slightly more conductive, so that electrical measurements could be performed with low noise. Two sets of electrodes (Al and Pt) were evaporated on the single crystal to form the first sample, schematically shown in Fig. 3(a). The I–V data are presented in Fig. 3(c). As indicated in the Ellingham diagram in Fig. 2(a), Al can significantly reduce TiO_2 to generate a large amount of oxygen vacancies at the Al/TiO_2 interface, while the Pt electrode does not. Therefore, a linear I–V was obtained between two Al electrodes, reflecting an Ohmic contact at the Al/TiO_2 interface. A rectifying I–V was obtained between an Al electrode and a Pt electrode as a result of the Schottky contact [28] formed at the metal/single-crystal semiconductor interface, i.e., the Pt/rutile TiO_2 interface, which is given as the red I–V in Fig. 3(c) (Pt electrode grounded). In order to show that even a Pt/TiO_2 interface can be turned into an ohmic contact with a large amount of oxygen vacancies, we prepared a second single-crystal sample. More oxygen vacancies were introduced to this rutile crystal by annealing it in vacuum at a higher temperature (800°C) and for a longer time (60 min). The crystal became dark blue after annealing, indicating a large concentration of oxygen vacancies. Then Al and Pt electrodes were evaporated onto the crystal. A linear I–V (cyan in Fig. 3(c)) was obtained even between the two Pt electrodes from this sample. These results confirmed that fewer oxygen vacancies at the metal/TiO_2 interface lead to a rectifying and resistive contact, while more oxygen vacancies result in a linear and conductive contact.

Controlling the interfacial concentration of oxygen vacancies can be used in device engineering and design. For

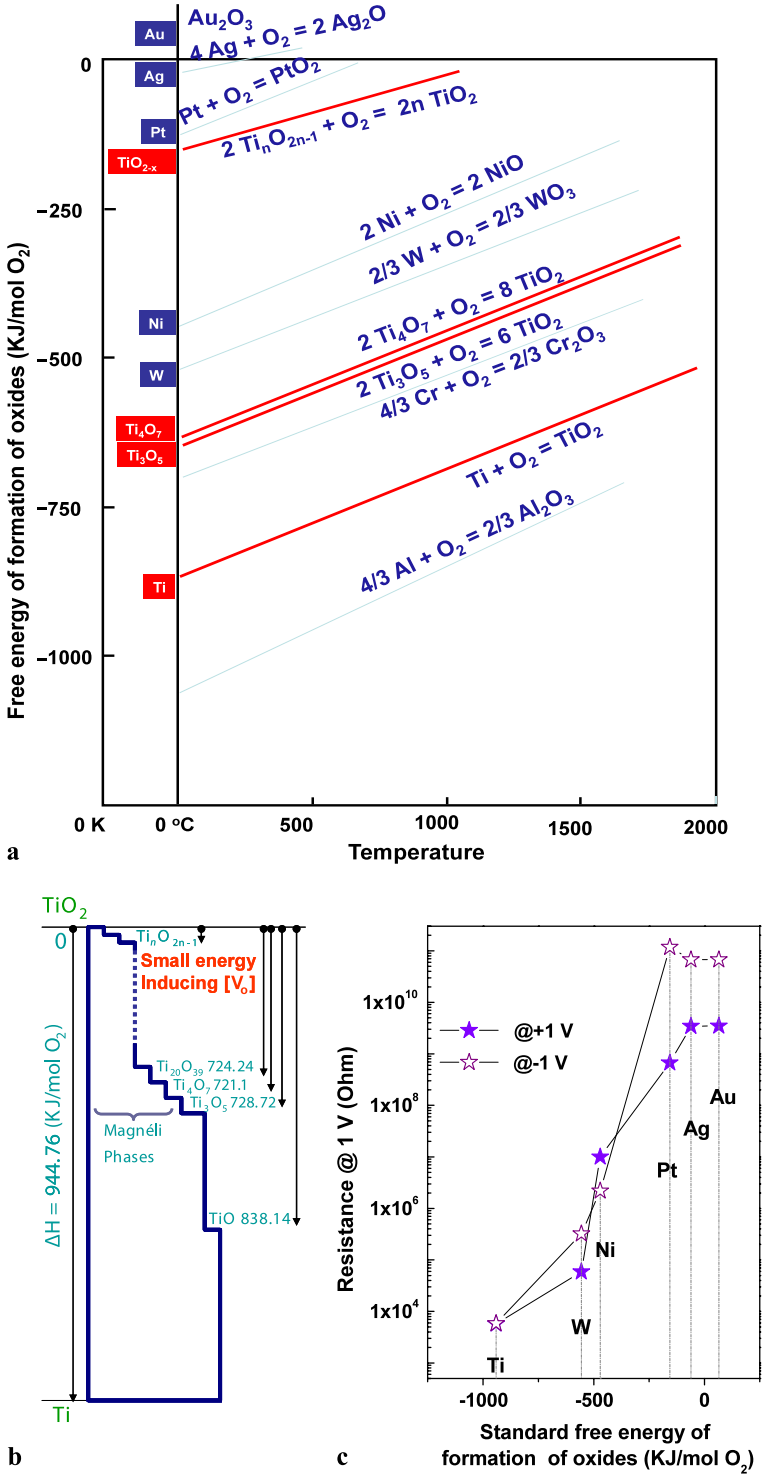

Fig. 2 (**a**) Ellingham diagram with different TiO_2 formation reactions from its sub-oxides. (**b**) Schematic of free energy steps for TiO_2 reduction reactions to its different sub-oxides. (**c**) A plot of device resistances at ±1 V vs. the standard free energy of formation of the metal electrode oxide

example, an asymmetry between the two interfaces in the metal/oxide/metal structure is very helpful in obtaining a repeatable switching behavior with well-defined switching polarity [4, 26], where the oxygen vacancy rich interface can serve as a reservoir of the mobile ions and the switching occurs at the relatively oxygen vacancy poor interface. Since the interface reactions between the top metal electrodes and the oxide essentially take place at ambient temperature (except for some heating caused by e-beam depositions), the thickness of the interfacial layer is expected to be comparable to or less than that of the native oxide on the surface of a metal. Depending on the material system, a ternary compound may form at the interface [20].

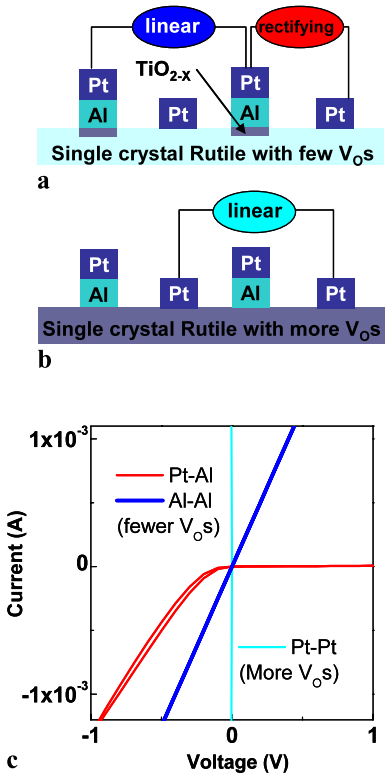

Fig. 3 Device schematics using TiO_2 rutile single crystals annealed slightly to generate a few oxygen vacancies (**a**) and annealed heavily to generate a large amount of oxygen vacancies (**b**). I–V plots obtained from the devices using the single crystals (**c**)

In conclusion, we have demonstrated that the thermodynamics of the metal/oxide interface plays a crucial role in TiO_2-based memristive device characteristics. Only the noble metals Au and Ag do not induce some oxygen vacancies at the interface. Other metals, including W and Ni, chemically reduce TiO_2 and create a significant concentration of oxygen vacancies, which dramatically reduces the electronic barrier at the interface and results in a conductive contact. These interface reactions dominate other factors, such as the work function of the electrode metal, in determining the device properties.

Acknowledgements We acknowledge J. Borghetti, X. Li, T. Ha and C. Le for excellent experimental assistance. This work is supported in part by the US Government's Nano-Enabled Technology Initiative.

References

1. L.O. Chua, IEEE Trans. Circuit Theory **CT-18**, 507 (1971)
2. L.O. Chua, S.M. Kang, Proc. IEEE **64**, 209 (1976)
3. D.B. Strukov, G.S. Snider, D.R. Stewart, R.S. Williams, Nature **453**, 80 (2008)
4. R. Waser, R. Dittmann, G. Staikov, K. Szot, Adv. Mater. **21**, 2632 (2009)
5. A. Sawa, Mater. Today **11**, 28 (2008)
6. J.J. Yang, M.D. Pickett, X. Li, D.A.A. Ohlberg, D.R. Stewart, R.S. Williams, Nat. Nanotechnol. **3**, 429 (2008)
7. D.H. Kwon, K.M. Kim, J.H. Jang, J.M. Jeon, M.H. Lee, G.H. Kim, X.S. Li, G.S. Park, B. Lee, S. Han, M. Kim, C.S. Hwang, Nat. Nanotechnol. **5**, 148 (2010)
8. Y.C. Yang, F. Pan, Q. Liu, M. Liu, F. Zeng, Nano Lett. **9**, 1636 (2009)
9. S.H. Jo, W. Lu, Nano Lett. **8**, 392 (2008)
10. M.J. Lee, S. Seo, D.C. Kim, S.E. Ahn, D.H. Seo, I.K. Yoo, I.G. Baek, D.S. Kim, I.S. Byun, S.H. Kim, I.R. Hwang, J.S. Kim, S.H. Jeon, B.H. Park, Adv. Mater. **19**, 73 (2007)
11. S.H. Jo, K.H. Kim, W. Lu, Nano Lett. **9**, 870 (2009)
12. Q. Liu, W.H. Guan, S.B. Long, R. Jia, M. Liu, J.N. Chen, Appl. Phys. Lett. **92**, 3 (2008)
13. B.J. Choi, D.S. Jeong, S.K. Kim, C. Rohde, S. Choi, J.H. Oh, H.J. Kim, C.S. Hwang, K. Szot, R. Waser, B. Reichenberg, S. Tiedke, J. Appl. Phys. **98**, 033715 (2005)
14. B. Gao, B. Sun, H.W. Zhang, L.F. Liu, X.Y. Liu, R.Q. Han, J.F. Kang, B. Yu, IEEE Electron Device Lett. **30**, 1326 (2009)
15. J. Borghetti, G.S. Snider, P.J. Kuekes, J.J. Yang, D.R. Stewart, R.S. Williams, Nature **464**, 873 (2010)
16. T. Hasegawa, T. Ohno, K. Terabe, T. Tsuruoka, T. Nakayama, J.K. Gimzewski, M. Aono, Adv. Mater. **22**, 1831 (2010)
17. H. Choi, H. Jung, J. Lee, J. Yoon, J. Park, D.J. Seong, W. Lee, M. Hasan, G.Y. Jung, H. Hwang, Nanotechnology **20**, 5 (2009)
18. Q.F. Xia, W. Robinett, M.W. Cumbie, N. Banerjee, T.J. Cardinali, J.J. Yang, W. Wu, X.M. Li, W.M. Tong, D.B. Strukov, G.S. Snider, G. Medeiros-Ribeiro, R.S. Williams, Nano Lett. **9**, 3640 (2009)
19. J. Borghetti, Z.Y. Li, J. Straznicky, X.M. Li, D.A.A. Ohlberg, W. Wu, D.R. Stewart, R.S. Williams, Proc. Natl. Acad. Sci. USA **106**, 1699 (2009)
20. H.Y. Jeong, J.Y. Lee, S.Y. Choi, Adv. Funct. Mater. **20**, 3912 (2010)
21. J.J. Yang, F. Miao, M.D. Pickett, D.A.A. Ohlberg, D.R. Stewart, C.N. Lau, R.S. Williams, Nanotechnology **20**, 215201 (2009)
22. J.P. Strachan, M.D. Pickett, J.J. Yang, S. Aloni, A.L.D. Kilcoyne, G. Medeiros-Ribeiro, R.S. Williams, Adv. Mater. **22**, 3573 (2010)
23. J.J. Yang, J. Borghetti, D. Murphy, D.R. Stewart, R.S. Williams, Adv. Mater. **21**, 3754 (2009)
24. E. Linn, R. Rosezin, C. Kugeler, R. Waser, Nat. Mater. **9**, 403 (2010)
25. M. Mrovec, J.M. Albina, B. Meyer, C. Elsässer, Phys. Rev. B **79**, 245121 (2009)
26. J.J. Yang, J.P. Strachan, Q. Xia, D.A.A. Ohlberg, P.J. Kuekes, R.D. Kelley, W.F. Stickle, D.R. Stewart, G. Medeiros-Ribeiro, R.S. Williams, Adv. Mater. **22**, 4034 (2010)
27. B.M. Herbert, J. Appl. Phys. **48**, 4729 (1977)
28. R.T. Tung, Mater. Sci. Eng., R Rep. **35**, 1 (2001)
29. C. Park, Y. Seo, J. Jung, D.W. Kim, J. Appl. Phys. **103**, 054106 (2008)
30. S.M. Sze, K.K. Ng, *Physics of Semiconductor Devices*, 3rd edn. (Wiley, New York, 2007)
31. J.P. Strachan, J.J. Yang, R. Munstermann, A. Scholl, G. Medeiros-Ribeiro, D.R. Stewart, R.S. Williams, Nanotechnology **20**, 485701 (2009)
32. R. Münstermann, J.J. Yang, J.P. Strachan, G. Medeiros-Ribeiro, R. Dittmann, R. Waser, Phys. Status Solidi RRL **4**, 16 (2009)
33. Y.A. Chang, W.A. Oates, *Materials Thermodynamics* (Wiley, New York, 2010)
34. P. Waldner, G. Eriksson, Calphad **23** 189 (1999)
35. J.J. Yang, N.P. Kobayashi, J.P. Strachan, D.A.A. Ohlberg, M.D. Pickett, Z. Li, G. Medeiros-Ribeiro, R.S. Williams, Chem. Mater **23**, 123 (2011)